

Lawrence Berkeley National Laboratory

LBL Publications

Title

Thermodynamic analysis of a novel fossil-fuel-free energy storage system with a trans-critical carbon dioxide cycle and heat pump

Permalink

<https://escholarship.org/uc/item/3hh9c0n0>

Journal

International Journal of Energy Research, 44(10)

ISSN

0363-907X

Authors

Hao, Yinpeng
He, Qing
Liu, Wenyi
et al.

Publication Date

2020-08-01

DOI

10.1002/er.5130

Peer reviewed

Thermodynamic Analysis of a Novel Fossil-Fuel-Free Energy Storage System with a Trans-Critical Carbon Dioxide Cycle and Heat Pump

Yinping Hao^{a,b}, Qing He^{a,*}, Wenyi, Liu^a, Lehua Pan^b,

Curtis M. Oldenburg^b

^aSchool of Energy Power and Mechanical Engineering, North China Electric Power University, No.2 Beinong Road, Changping, Beijing 102206, China

^bEnergy Geosciences Division, 74-316C, Lawrence Berkeley National Laboratory, Berkeley, CA 94720, USA

Abstract: This paper presents and analyzes a novel fossil-fuel-free trans-critical energy storage system that uses CO₂ as the working fluid in a closed loop shuttled between two saline aquifers or caverns at different depths, one a low-pressure reservoir, and the other a high-pressure reservoir. Thermal energy storage and a heat pump are adopted to eliminate the need for external natural gas for heating the CO₂ entering the energy recovery turbines. We carefully analyze the energy storage and recovery processes to reveal the actual efficiency of the system. We also highlight thermodynamic and sensitivity analyses of the performance of this fossil-fuel-free trans-critical energy storage system based on a steady-state mathematical method. It is found that the fossil-fuel-free trans-critical CO₂ energy storage system has good comprehensive thermodynamic performance. The exergy efficiency, round-trip efficiency, and energy storage efficiency are 67.89%, 66% and 58.41%, and the energy generated of per unit storage volume is 2.12 kW·h/m³, and the main contribution to exergy destruction is the turbine re-heater, from which we can quantify how performance can be improved. Moreover, with a relatively higher energy storage and recovery pressure and lower pressure in the low-pressure reservoir, this novel system shows promising performance.

Keywords: fossil-fuel-free, compressed trans-critical CO₂, subsurface energy storage, heat pump, thermodynamic analysis, sensitivity analysis

Note: This is the manuscript form of a published paper and may differ slightly from the final published paper. Please read and cite the final published paper:

Hao, Y., He, Q., Liu, W., Pan, L. and Oldenburg, C.M., Thermodynamic analysis of a novel fossil-fuel-free energy storage system with a trans-critical carbon dioxide cycle and heat pump. *International Journal of Energy Research*.

*Corresponding author:
E-mail address: hqng@163.com (Qing He).

38 **1. Introduction**

39 Increasing energy demand and rising concern about greenhouse gas emissions
40 from fossil-fuel power generation have led to worldwide interest in renewable energy
41 sources [1]. Rapid development and worldwide utilization of renewable energy sources
42 bring not only diversification of the global energy industry, but also challenges in
43 integrating renewable energy such as wind and solar energy into the electricity grid due
44 to intermittency and instability over a wide range of time scales from short (minute) to
45 long (seasonal) [2-5]. In order to optimize integration of wind and solar power into the
46 electricity grid, practical large-scale (bulk) energy storage systems (ESS) are urgently
47 needed. The technologies currently are available to provide bulk energy storage include
48 pumped hydro storage (PHS) and compressed air energy storage (CAES) [6-8]. The
49 development of batteries for bulk energy storage is ongoing, but there are only a few
50 utility-scale stationary battery storage projects in place for long-term (daily) storage
51 and these systems are expensive and provide only a small fraction of energy stored by
52 pumped hydro storage [9,10].

53 It is well known that the only two current operating conventional CAES plants rely
54 on natural gas for energy recovery resulting in greenhouse gas emissions. The fact that
55 renewable energy stored by CAES may result in greenhouse gas emissions upon energy
56 recovery has motivated thinking about novel CAES systems, some of which can avoid
57 the need for natural gas. Among the many novel CAES systems that have been proposed
58 are the super-critical CAES (SC-CAES) [11], porous media CAES (PM-CAES) [12],
59 and small scale CAES [13]. In addition, several new approaches to adiabatic CAES
60 have recently been introduced. For example, advanced adiabatic CAES (AA-CAES)
61 [14-16] and high-temperature adiabatic CAES [17] have been analyzed and show
62 potential to solve the economic and environmental challenges related to the use of fossil
63 fuel combustion during energy recovery. Thermodynamic analyses have become
64 standard for these systems for design and efficiency analyses [18-20]. Several of new
65 CAES systems [21, 22] have been proposed to improve thermal efficiency of CAES,

66 and liquefied air energy storage (LAES) [23, 24] has been studied to improve energy
67 storage density.

68 Recently, growing interest has been focused on the use of carbon dioxide (CO₂) in
69 compressed gas storage because of its unique properties and characteristics. Utilizing
70 CO₂ instead of air in compressed gas energy storage will not only improve the system
71 performance but also offer a possibility for utilization of CO₂ with corresponding
72 reductions in carbon emission [25]. Wu et al. [26] proposed a novel trans-critical
73 compressed CO₂ energy storage system that showed good performance, energy storage
74 density, and high efficiency. Liu et al. [27] proposed a system that combined
75 compressed gas energy storage in deep subsurface reservoirs (porous media or caverns)
76 and utilization of CO₂ which gets much higher energy density and good energy storage
77 efficiency. Buscheck et al. [28] were investigating ways to exploit deep reservoirs for
78 both their ability to store CO₂ beneficially in both the geologic carbon sequestration
79 context and for energy storage, including exploitation of natural geothermal heating of
80 the CO₂. Ahmadi et al [29-32] explored a few of novel CO₂ power cycles and
81 thermodynamic optimizations on these systems have been performed. Mehmet et al.
82 [33] posed novel electro-thermal energy storage with trans-critical CO₂ cycles, aiming
83 to make improvement on the CO₂ machines and the system performance. An
84 optimization on thermodynamic performance of the turbine turbomachinery in an
85 energy storage system with CO₂ as working fluid has been performed [34]. Based on
86 CO₂ in a Brayton cycle, a compressed CO₂ energy storage cycle has been proposed and
87 thermodynamic optimization showed much better thermal performance compared with
88 other CAES systems [35].

89 Based on the above research, the development of compressed gas energy storage
90 utilizing CO₂ as working fluid has become a focus of research and development. In this
91 paper, we present and analyze a novel closed-loop energy storage system that uses CO₂
92 as the working fluid that is cycled between high-pressure and low-pressure reservoirs.
93 The innovation highlight in this system is that we analyze the use of a heat pump instead
94 of fossil fuel to recover and reheat stored heat of compression during the energy
95 recovery process. We present mathematical thermodynamic models of the proposed

96 compressed trans-critical CO₂ energy storage system, and carry out parametric analyses
97 to examine the effects on system performance of key thermodynamic parameters.

98 **2. System description**

99 We propose a closed-loop energy storage system that takes advantage of the large
100 volumes and remote subsurface locations of saline aquifers or large storage caverns for
101 hosting two CO₂ storage reservoirs. One reservoir is low-pressure, and the other is high-
102 pressure, which serve to store, respectively, CO₂ entering the electricity-producing
103 turbines, and CO₂ following compression in the storage cycle. In this novel energy
104 storage system, the CO₂ transitions from supercritical state to gaseous state in the
105 turbines, which is denoted as a trans-critical compressed CO₂ energy storage (TC-
106 CCES). The schematic of this novel TC-CCES is depicted in Fig. 1, and its T-S graph
107 is illustrated in Fig. 2. The schematic of the heat pump sub-system of the TC-CCES
108 system is shown in Fig. 3.

109 **2.1 Energy storage process**

110 As shown in Fig. 1, the green background represents the energy storage process
111 (compression phase), and the orange background represents the energy recovery
112 process (generation phase). The overlapping region in the middle includes the heat
113 storage unit, cold storage unit, and low- and high-pressure reservoirs (LR and HR), all
114 of which are involved in both energy storage and energy recovery process.

115 The working principle of the storage process is as follows:

116 (a) 14-1: The working fluid (trans-critical CO₂) stored in LR is cooled through a
117 pre-cooler (PC) and injected into the compressor, with the heat of compression (19-20)
118 stored in the heat storage unit.

119 (b) 1-2, 3-4, 5-6: During hours when excess renewable electricity is available, the
120 CO₂ is pressurized in the compressor to temperatures and pressures above the critical
121 point (304.15K, 7.4 MPa).

122 (c) 2-3, 4-5: The compressed CO₂ heats up in the process, and is then cooled by
123 the inter-cooler heat exchangers (IC1 and IC2), and the heat generated during the

124 compression process (15-16, 17-18) is stored in the heat storage unit.

125 (d) 6-7: The compressed CO₂ with high temperature and pressure then is directly
126 injected into HR for storage.

127 **2.2 Energy recovery process**

128 The working principle of the recovery process is as follows:

129 (a) 7-8: CO₂ at high temperature and high pressure, potentially with additional
130 geothermal heat absorbed from the deep reservoir, is adjusted to a fixed pressure
131 through the high-pressure valve, and is fed into the energy recovery turbine.

132 (b) 8-9, 10-11, 12-13: The high-pressure CO₂ powers the turbines resulting in
133 strong cooling of the CO₂, which is then fed into LR.

134 (c) 9-10, 11-12: The CO₂ exhausted from the turbines in front (8-9 or 10-11) is too
135 cold to feed the next turbines (10-11 or 12-13). This exhausted CO₂ is reheated in TR1
136 or TR2 to prevent liquid CO₂ from forming and to provide enough volume throughput
137 to drive each turbine. This reheating is accomplished using the heat provided by the hot
138 water from the heat storage unit added by the heat pump system.

139 (d) 22-23: The temperature of the hot water stored in the heat storage unit (21-22)
140 after absorbing the CO₂ compression heat is not high enough to reheat the exhausted
141 CO₂ in the generation turbine train. Therefore, the hot water withdrawn from the heat
142 storage unit is further heated by means of the heat pump (27-23) to raise its temperature
143 to a required level. This heat pump is the key new feature of the system included to
144 obviate the need for natural gas in the energy recovery process.

145 **2.3 Heat pump system**

146 The term high-temperature heat pump (HTHP) is frequently used in connection
147 with industrial heat pumps, mainly for waste heat recovery in process heat supply [36].
148 In the compression system proposed here, the temperature of the heat storage unit would
149 not be sufficient to maintain CO₂ pressure after exiting from Turbine 1 to drive Turbine
150 2, and similarly for exiting from Turbine 2 to drive Turbine 3 to generate electricity.
151 What is needed is a way to transfer the waste heat stored in the heat storage unit which
152 is at approximately 383K into the exhaust streams of the turbines which are at a

153 temperature of approximately 363K. Due to the relatively high inlet temperature
154 (approximately 423K) of Turbine 2, a heat pump is needed to make full use of the stored
155 waste heat.

156 In selecting a working fluid for the heat pump, we prioritized efficient and steady
157 performance along with low environmental impact factor and high safety. We found
158 that R245fa is a low-pressure, high-temperature, and environmentally safe fluid with a
159 high enough critical temperature (427K) for use as the heat pump working fluid [36,
160 37]. We evaluated the thermodynamic properties of R245fa using PEFPROP [38]. The
161 physical properties of R245fa are given in Table 1. The schematic of the heat pump is
162 illustrated in Fig. 3. The working principle of the heat pump can be described as:

163 (a) 29-30: R245fa is compressed during a non-isentropic process.

164 (b) 30-31: Gaseous high-pressure R245fa is cooled by hot water from the heat
165 storage unit (22) resulting in condensation that provides latent heat to the water exiting
166 (23) to the turbine exhaust heating loop at a specified temperature (433.15K).

167 (c) 31-32: Liquid R245fa expands through the expansion valve in a non-isentropic
168 process.

169 (d) 32-29: Liquid R245fa is heated through the evaporator by water from the
170 turbine exhaust cooling loop (27) causing R245fa to vaporize and causing cooling of
171 the water that exits to the ‘cold’ water storage tank.

172 **3. Theoretical model**

173 For simplicity, we make the following assumptions about the proposed TC-CCES:

174 (a) The TC-CCES system uses the thermodynamic model based on the
175 thermodynamic law and operates at steady-state conditions, and we ignore pressure
176 drops and heat losses in the pipes, heat exchangers, heat storage tank, and heat pump.
177 The water stored in the cold storage unit will be cooled down to room temperature
178 (298.15K) before it is used to cool the CO₂ from LS being fed to the compressor train.

179 (b) Equal CO₂ mass flow rates are assumed during the energy storage process
180 (withdrawing CO₂ from the LR and injecting CO₂ at high-pressure into the HR) and the
181 energy recovery process (withdrawing high-pressure CO₂ from the HR and injecting

182 low-pressure CO₂ into the LR).

183 (c) The system is closed (there are no losses of CO₂ within the storage reservoirs or
184 in the above-ground facility) and the stored energy of compression is large enough that
185 we can neglect kinetic and potential energy changes as CO₂ flows through the closed-
186 loop system. In addition, the details of wellbore flow are ignored in the analysis and we
187 assume constant wellhead P-T conditions during withdrawal and injection periods.

188 3.1 Compressor train

189 The compressors used for storing energy have isentropic efficiencies given by

$$190 \quad \eta_c = \frac{h_{i,s}'' - h_i'}{h_i'' - h_i'} \quad (1)$$

191 where, h_i' is the enthalpy of inlet compressor; $h_{i,s}''$ is the isentropic enthalpy of outlet
192 compressor; h_i'' is the real enthalpy of outlet compressor; and i is the stage of
193 compressor train, $i = 1, 2, 3$.

194 The power consumed by compression $W_{c,i}$ is

$$195 \quad W_{c,i} = h_i'' - h_i' \quad (2)$$

196 3.2 Turbine train

197 The turbines used for recovering energy have efficiencies and power needs
198 analogous to those of the compressors. The isentropic efficiency of expansion in the
199 turbine η_T is

$$200 \quad \eta_T = \frac{h_j' - h_{j,s}''}{h_j' - h_j''} \quad (3)$$

201 where, h_j' is the enthalpy of inlet turbine; $h_{j,s}''$ is the isentropic enthalpy of the outlet
202 turbine; h_j'' is the real enthalpy of the outlet turbine; and j is the stage of the turbine
203 train, $j=1, 2, 3$.

204 The power output during expansion by the turbine $W_{T,j}$ is

$$205 \quad W_{T,j} = h_j' - h_j'' \quad (4)$$

206 3.3 Storage model

207 For a saline aquifer storage reservoir, the groundwater in the aquifer has a pressure

208 P_{hs} given by

$$209 \quad P_{hs} = \rho_w g Z \quad (5)$$

210 The LR is envisioned to be located at a shallower depth than the HR because the
211 CO₂ well bottom pressure must exceed the reservoir pressure for injection to occur.
212 Cavern pressures are more flexible, and there are no a priori restrictions on the depths
213 of the low- and high-pressure reservoirs for caverns.

214 Similar to pressure, temperature increases with depth as given by the geothermal
215 gradient, G , making T at any depth given by

$$216 \quad T = T_s + GZ \quad (6)$$

217 where, T_s is the temperature at the ground surface.

218 To estimate saline aquifer reservoir volume, V_s is calculated from the following
219 equations,

$$220 \quad V_s = \frac{M_{CO_2}}{(\rho'_{CO_2} - \rho''_{CO_2})} \quad (7)$$

221 3.4 Heat exchanger model

222 Both inter coolers and heaters of this system are applicable to the following model.
223 The model for the heat-exchange processes involving CO₂ must be divided up into
224 small steps to accommodate the large changes in CO₂ properties that occur as the
225 temperature changes around the CO₂ critical point [39]. In the inter cooler between two
226 compressors, the working fluid on the hot-stream side and cold-stream side are CO₂ and
227 water, respectively. We suppose that the temperature difference ΔT on the hot-stream
228 side is fixed and separated into N equal parts. Therefore, the heat transfer rate for the k -
229 th part and mass flow rate of water can be illustrated below,

$$230 \quad \dot{Q}_{he,k} = \dot{m}_{CO_2} C_{p,CO_2,k} (T_{CO_2,k} - T_{CO_2,k+1}) \quad (8)$$

$$231 \quad \dot{Q}_{he,k} = \dot{m}_w C_{p,w,k} (T_{w,k+1} - T_{w,k}) \quad (9)$$

232
$$\dot{m}_w = \frac{\sum_k^N \dot{Q}_{he,k}}{(h_{w,out} - h_{w,in})} \quad (10)$$

233 **3.5 Heat pump system**

234 The high-temperature heat pump system is composed of a compressor, a condenser,
235 an expansion valve, and an evaporator.

236 **3.5.1 Compressor**

237 Similar to the energy storage compressor, but with R245fa as working fluid instead
238 of CO₂, the principal calculation is the same as that of energy storage compressor.

239 **3.5.2 Condenser**

240 In the heat pump condenser, the working fluids on both the hot-stream side and
241 cold-stream side are R245fa and water, respectively. The mass flow rate of water is
242 modeled by the equations

243
$$\dot{Q}_{he} = \dot{m}_{R245fa} C_{p,R245fa} (T'_{R245fa} - T''_{R245fa}) \quad (11)$$

244
$$\dot{Q}_{he} = \dot{m}_w C_{p,w} (T''_w - T'_w) \quad (12)$$

245
$$\dot{m}_w = \frac{\dot{Q}_{he}}{(h''_w - h'_w)} \quad (13)$$

246 **3.5.3 Evaporator**

247 In the evaporator of heat pump, R245fa is on the cold-stream side and water is on
248 the hot-stream side. The principal calculation is the same as that of the condenser of the
249 heat pump, except that the hot and cold streams are swapped.

250 **3.5.4 Expansion valve**

251 The expansion valve expands and depresses in the heat pump system and the
252 entropies in the front and rear valves are equal, so the power is zero.

253 **4. Performance criteria**

254 To evaluate and compare the performance of the proposed TC-CCES system, we
255 calculate the energy round-trip efficiency, energy storage efficiency, exergy efficiency,
256 and energy generated per unit volume as quantities indicative of performance [40, 41].

257 **4.1 Energy analysis**

258 **4.1.1 Round-trip efficiency**

259 In general, for an energy cycle, the round-trip efficiency is often used to measure
260 the performance of power unit that has an energy storage component. Round-trip
261 efficiency is defined as the ratio of the electricity output during the recovery phase over
262 the sum of the electricity consumed during the storage phase and the electricity (or
263 equivalent energy) consumed during recovery phase [41], specifically,

$$264 \quad \eta_{RT} = \frac{E_T}{E_C + \sum E_i} \quad (14)$$

265 where, E_T is the electricity output in the energy recovery process; E_C represents the
266 total energy consumed during the energy storage process, and $\sum E_i$ is the electricity
267 (or equivalent energy, e.g., natural gas converted into electricity in a conventional
268 CAES power plant) consumed in the recovery process.

269 In the TC-CCES presented here, the latter term in Eq. (14) is the electricity used
270 to power the heat pump.

271 **4.1.2 Energy storage efficiency**

272 While round-trip efficiency is a useful measure of the efficiency of a power plant
273 with storage component, it is not a direct measurement of storage efficiency, i.e., how
274 much stored energy can be recovered, because the large portion of electricity output
275 may come from added natural gas during recovery in a conventional CAES system. As
276 a result, it may be misleading to compare the efficiency of a CAES system against a
277 battery-based electricity storage system using round-trip efficiency because the natural
278 gas added during recovery in a conventional CAES system is really not a part of storage.
279 To facilitate the comparison of storage efficiency across different type storage systems,
280 we introduce a new performance criterion, named energy storage efficiency, which is

281 defined as the ratio of the net energy that can be recovered from the system over the
 282 energy that consumed during storage:

$$283 \quad \eta_{ES} = \frac{E_T - \sum E_i}{E_C} \quad (15)$$

284 where, $E_T - \sum E_i$ is the net energy recovered from storage process.

285 4.1.3 Energy generated per unit volume

286 The energy generated per unit volume of storage (EGV) for a TC-CCES system
 287 with two saline reservoirs is

$$288 \quad EGV = \frac{E_{GEN}}{V_s} = \frac{W_T \cdot t_{recovery}}{V_s} \quad (16)$$

289 4.2 Exergy analysis

290 Approaches for improving the performance of the system can be found by energy
 291 flow analysis. Therefore, we have carried out an exergy analysis to calculate exergy
 292 destruction in the TC-CCES system and its components.

293 The n^{th} component of the system can be described by its exergy balance equation
 294 [42, 43]

$$295 \quad \dot{E}_{d,n} = \dot{E}_{F,n} - \dot{E}_{P,n} \quad (17)$$

296 where, $\dot{E}_{d,n}$, $\dot{E}_{F,n}$ and $\dot{E}_{P,n}$ are the exergy destruction rate, fuel exergy rate, and the
 297 product exergy rate, respectively.

298 We define exergy efficiency as

$$299 \quad \eta_{EX} = \frac{E_P}{E_F} \quad (18)$$

300 The equations we use to calculate the component-by-component exergy
 301 destruction are listed in Table 2. Each component (n) of the system has an exergy
 302 destruction ratio defined as

$$303 \quad X_{d,n}^* = \frac{\dot{E}_{d,n}}{\dot{E}_{F,n}} \quad (19)$$

304 **5. Results and discussion**

305 The properties of the system as summarized in Table 3 were used for the
306 simulations and parametric analysis.

307 **5.1 Thermodynamic analysis**

308 Due to the use of an underground gas storage environment in the TC-CCES system,
309 the temperature of CO₂ stored in HR may change in three different ways depending on
310 the local geothermal gradient. (1) CO₂ could gain geothermal energy from the rock and
311 become hotter; (2) heat stored in the CO₂ could be absorbed by rock in the HR region
312 and cool; or (3) the CO₂ may neither gain nor lose heat and instead stay at approximately
313 the same temperature. The thermodynamic analysis presented here assumes the first
314 case because HR is likely to be deep whether it is an aquifer or a cavern. The analysis
315 results of the TC-CCES system with heat pump are presented in Table 4, and the results
316 of the power of compressors, turbines and heat pump are shown in Table 5. The results
317 of the system efficiency and EGV are shown in Table 6. A summary of the results of
318 performance criteria of the TC-CCES system and the results in [27] are shown in Table
319 7. The value of η_{RT} and η_{EX} of the TC-CCES system are 66.00% and 67.89%,
320 respectively, which are better than the corresponding 63.35% and 53.02% in [27]. In
321 particular, we find the value of η_{ES} is 58.41%, which is almost three times that in [27].
322 We also find that the energy generated per unit storage volume (EGV) of this novel TC-
323 CCES system is 2.12 kW·h/m³, lower than that in [27], which is 3.07 kW·h/m³. The
324 reason can be explained from Table 7. From the data on power distribution in energy
325 recovery process in [27], the power output of the turbine train is derived from two

326 sources: (1) the energy stored by the compression process, and (2) the energy supplied
327 by extra fuel to heat the cold turbine output gas. The total power output of the turbine
328 train is 254.82 kW, and the extra fuel input is 217.86 kW, which accounts for 85.5% of
329 the whole power output, so the net electricity power supplied by the storage process is
330 very low, only 36.96 kW, which accounts for 14.5% of the total power output.
331 Meanwhile, the utilization rate of fuel exergy is as high as 89%. In the novel TC-CCES
332 system with heat pump, no extra fuel energy is input during energy recovery process,
333 but the heat pump requires electricity power equal to 44.24 kW, which accounts for
334 28.1% of total output. During the turbine train work in the energy recovery process, and
335 the energy stored by the compression process is supplied to the turbine train making the
336 energy storage efficiency higher than in [27]. The utilization of heat exergy in TR is
337 55.1% because of the large use of fuel, the exergy utilization is higher than thermal for
338 the part of using turbine re-heater instead of fuel on the reheating the turbines process,
339 but energy storage efficiency, exergy efficiency and round-trip efficiency of the TC-
340 CCES system are larger than that in [27]. According to Eq. (7) and Eq. (16), the value
341 of EGV mainly depends on two parts: (1) the net electricity power output and (2) the
342 density difference between the inlet, and outlet CO₂ in the storage reservoir. In the prior
343 TC-CCES, the value of the density difference is much smaller than that in the TC-CCES
344 system. Hence, the value of EGV in [27] is larger than that in the TC-CCES system. In
345 order to use the TC-CCES, a large underground storage reservoir volume is needed,
346 consistent with use of an aquifers or solution-mined caverns.

347 The exergy destruction percentages for the various system components are
348 depicted in Fig. 4. From Fig. 4, one sees for the TC-CCES system that 44.91% of the

349 irreversibility occurs in TR, 20.46% in HP, 16.63% in IC, 4.95% in C, 4.41% in T, 4.13%
350 in HR, 3.17% in PC, and 1.32% in LR.

351 **5.2 Sensitivity analysis**

352 From the thermodynamic performance analysis, we find the novel TC-CCES
353 system has high exergy efficiency, energy storage efficiency and round-trip efficiency.
354 The main properties controlling the efficiency and EGV of the system are, the energy
355 storage pressure (inlet pressure of HR), energy recovery pressure (inlet pressure of the
356 T1), and pressure of the LR (outlet pressure of the T3) [44]. We conducted a sensitivity
357 analysis with parameter ranges listed in Table 8 to quantify how performance can be
358 improved.

359 **5.2.1 Effect of energy storage pressure**

360 It is noted that the pressure drop across the high-pressure throttle valve maintains
361 2 MPa and stays almost constant. When the energy storage pressure varies from 15 MPa
362 to 25 MPa, the energy recovery pressure will also change, varying from 13 MPa to 23
363 MPa with a 1 MPa increment, while the pressure of LR is set as 1 MPa, and other
364 parameters remain unchanged. As shown in Fig. 5, the overall pressure of the storage
365 system plays a large role in the TC-CCES efficiency. Specifically, the value of η_{RT} ,
366 η_{ES} , and η_{EX} increase as energy storage pressure increases. Note that there is a
367 crossover of η_{RT} and η_{EX} at a pressure of 20 MPa. This occurs because an increase
368 in the energy storage pressure leads to an increase of net energy output during the
369 energy recovery process, which can increase the value of EGV. The required volume of
370 the HR is reduced by high energy storage pressure, whereas variation of the power
371 output is contrary to that of the required volume. Hence, EGV will rise along with
372 increase of the energy storage pressure.

373 Fig. 6 depicts the changes in the power of the compressor train, turbine train, and
374 heat pump with the changes in energy storage pressure. As the energy storage pressure
375 increases, the output of the heat pump gently increases, whereas the net output of
376 compressor and turbine have stronger growth trends that level off at high pressures. The
377 reason why growth is gradually slowing down is that for the compressor train, as the

378 storage pressure increases, the CO₂ working fluid changes from a trans-critical state to
379 a supercritical state. Due to the physical properties of the supercritical CO₂ itself, the
380 power consumed by the compressor will reduce and the power output by the turbine
381 will reduce, so both growth rate of the power consumption of the compressor train and
382 output power of the turbine train gradually decreases. Energy storage pressure also
383 controls the exergy destruction percentage in the main components. In Fig. 7, it is seen
384 that exergy destruction occurs mainly in TR, HP, and IC, with the largest exergy
385 destruction coming from TR. The inlet pressure of the turbine will grow with the rise
386 of the energy storage pressure, and all other setting parameters held constant. Hence,
387 the temperature difference of the heat exchangers will grow, therefore, the exergy
388 destruction percentage increases from 62.42 kW to 83.89 kW in IC, and decreases from
389 184.6 kW to 176.3 kW in TR. The exergy destruction rate occurring in C, T, and HR
390 have a similar increasing trend with rise in energy storage pressure, which is caused by
391 the pressure difference between the inlet and outlet of each component; the higher the
392 pressure drop is, the larger the exergy destruction will become.

393 **5.2.2 Effect of energy recovery pressure**

394 It is noted that when the pressure of energy recovery changes from 8 MPa to 15
395 MPa with 1 MPa increment, the energy storage pressure and the pressure of LR are set
396 to 17 MPa and 1 MPa while the other setting parameters listed in Table 3 remain
397 unchanged. In Fig. 8 it is illustrated the dependence of η_{RT} , η_{ES} , and EGV with the
398 energy recovery pressure. The value of η_{ES} increases from 41.63% to 58.41%, the
399 value of η_{RT} rises from 52.54% to 62.16%, the value of η_{EX} has a gentle change from
400 66.9% to 68.87%. What's more, the growth in energy recovery pressure will result in a
401 rise in the output power of the turbine train, the pressure drop will decline which causes
402 a smaller volume required for HR. Therefore, the EGV will increase with higher energy
403 recovery pressure.

404 The effects of energy recovery pressure on the power in the compressor train,
405 turbine train and heat pump are shown in Fig. 9. The power of the compressor train is
406 constant and the power of the turbine train increases rapidly from 124.82 to 157.06 kW

407 with growth of the energy recovery pressure. In addition, the power of the heat pump
408 mainly depends on the amount of heat exchange required for the reheating of the turbine
409 during the energy recovery process, whereas it is independent of the energy recovery
410 pressure. Therefore, the heat pump power requirement is almost constant in the energy
411 recovery process.

412 Fig. 10 illustrates the influence of energy recovery pressure on the exergy
413 destruction rate of the system components. The exergy destruction rate of TR and PC
414 decline with larger energy recovery pressure in the TC-CCES system, which varies
415 from 186.1 kW to 183.6 kW in TR and 21.17 kW to 12.96 kW in PC. The reason is that
416 the exergy destruction of TR and PC are mainly controlled by their temperature
417 differences. In fact, the temperature differences across TR and PC will be smaller with
418 larger energy recovery pressure. Therefore, the exergy destruction in TR and PC will
419 be smaller for greater energy storage pressure in the case that all other parameters
420 remain unchanged. And it can be also found that the exergy destruction of other
421 components change only slightly with energy recovery pressure.

422

423 **5.2.3 Effects of pressure in LR**

424 When the pressure in the low-pressure reservoir has a change from 1 MPa to 2
425 MPa, with a 0.2 MPa increment, the energy storage pressure and energy recovery
426 pressure are set as 17 MPa and 15 MPa, respectively, and other setting parameters are
427 kept constant. In Fig. 11 it can be observed that as with higher pressure of LR, the values
428 of η_{RT} , η_{ES} , η_{EX} , and EGV of the TC-CCES system are reduced. The maximum
429 change is in η_{ES} which decreases from 58.41% to 37.6%, the second largest change is
430 in η_{RT} which reduces from 66.16% to 49.3%, the value of η_{EX} has a gentle decline
431 of 3.54%. When CO₂ in the LR is in a trans-critical state, the pressure change of LR has
432 a greater effect on the change of the CO₂ density, so the volume change of the gas
433 storage reservoir becomes larger, the EGV decreases larger. Fig. 12 shows the influence
434 of the pressure of LR on the power of the compressor train, turbine train, and heat pump.
435 With increase of pressure of the LR, the power of the turbine train decreases sharply
436 from 157.06 to 117.16 kW. The reason is that in the case of other design parameters

437 unchanged, the increase of pressure of LR causes the power of each stage of the turbine
438 to be reduced and the net output of the system to be reduced, while the consumption of
439 the system compressor remains constant.

440 The effects of the various components on exergy destruction rate as a function of
441 the pressure of LR are shown in Fig. 13. The analysis shows that the exergy destruction
442 rates of TR and PC rise with growing pressure of LR, which increases from 184.5 to
443 192 kW in TR and from 1.3 to 14 kW in PC. The reason for this increase is that the
444 outlet temperature of each turbine increases and the power of the turbine decreases with
445 higher LR pressure and therefore the exergy destruction of TR and PC increases. In
446 addition, the pressure difference becomes larger in LR, which varies from 5.4 to 46.1
447 kW, as pressure in LR increases, making the exergy destruction rate of LR increase.

448 **6. Conclusions**

449 This study contained a thermodynamic analysis of a novel, fossil-fuel-free, TC-
450 CCES system that uses two saline aquifers or caverns for storing compressed CO₂ and
451 that includes two thermal storage tanks and a heat pump system as thermal storage and
452 recovery systems, respectively and an investigation of its operational behavior and
453 efficiency. The main conclusions are:

454 (1) Under a typical trans-critical operation condition, the round-trip efficiency is
455 66%, energy storage efficiency is 58.41%, exergy efficiency is 67.89% and EGV is 2.12
456 kW·h/m³, which indicates a good thermodynamic performance of the novel TC-CCES
457 system.

458 (2) Sensitivity analysis shows that higher energy storage pressure, energy recovery
459 pressure and lower the pressure of LR will improve the four performance indicators
460 including η_{RT} , η_{ES} , η_{EX} and EGV.

461 (3) By comparing the exergy destruction rate of the main components in the system,
462 we find the exergy destruction rate of the heat exchangers accounts for a large
463 proportion of exergy destruction with 49.3% in TR and 16.46% in IC, respectively. It
464 indicates that significant potential improvement in system performance can be made by
465 optimizing the turbine re-heater exchanger to reduce the exergy destruction rate.

466 We note finally that the operating efficiency of the system is good, the working
467 parameters are not extreme during operation, and the requirements of the components
468 in the system are reasonable suggesting it may be practical to build and operate this
469 novel fossil-fuel-free trans-critical CO₂ energy storage system.

470 **Acknowledgements**

471 We thank the National Key Research and Development Program of China (Grant
472 No.2017YFB0903601), the Double First-rate Construction Program of China, and
473 Lawrence Berkeley National Laboratory supported by the U.S. Department of Energy
474 under Contract No.DE-AC02-05CH11231.

475 **References**

- 476 [1] Qin, J.X., The Status and Prospect of New Energy and Renewable Energy in China. Material
477 Science, Energy Technology and Power Engineering. 2018, Amer Inst Physics: Melville.
- 478 [2] P.S. Georgilakis, Technical challenges associated with the integration of wind power into power
479 system, *Renew. Sustain. Energy Rev.* 12 (2008) 852-863.
- 480 [3] Wang, J., Qin, S., Jin, S., Estimation methods review and analysis of offshore extreme wind
481 speeds and wind energy resources. *Renewable & Sustainable Energy Reviews*, 2015. 42: p. 26-
482 42.
- 483 [4] Świerczyński, M., Teodorescu, R., Rasmunssen, C., Overview of the energy storage systems for
484 wind power integration enhancement. *IEEE International Symposium on Industrial Electronics*.
485 2010.
- 486 [5] Chen, L., Dai, Y., Min, Y., Study on the Mechanism of Transient Voltage Stability of Wind Power
487 With Power Electronic Interface. 2015 *IEEE Pes Asia-Pacific Power and Energy Engineering*
488 *Conference*. 2015, New York.
- 489 [6] Castillo A, Gayme D F. Grid-scale energy storage applications in renewable energy integration:
490 A survey[J]. *Energy Conversion and Management*, 2014, 87:885-894.
- 491 [7] B. Dursun, S. Alboyaci. The contribution of wind-hydro pumped storage systems in meeting
492 Turkey's electric energy demand, *Renew. Sustain. Energy Rev*, 14 (2010) 1979-1988.
- 493 [8] I. Arsie, V. Marano, G. Nappi, G. Rizzo. A model of hybrid power plant with wind turbines and
494 compressed air energy storage, in: *Proceedings of the ASME Industrial Power Conf. Pts A and*
495 *B*, 2005, pp.987-1000.
- 496 [9] Aneke, M. and Wang, M. Energy storage technologies and real life applications—A state of the
497 art review. *Applied Energy*, 2016,179, pp.350-377.
- 498 [10] Temple, J. The \$2.5 trillion reason we can't rely on batteries to clean up the grid, *MIT*
499 *Technology Review*, 2018, July 27, 2018. [https://www.technologyreview.com/s/611683/the-
500 25-trillion-reason-we-cant-rely-on-batteries-to-clean-up-the-grid/](https://www.technologyreview.com/s/611683/the-25-trillion-reason-we-cant-rely-on-batteries-to-clean-up-the-grid/)
- 501 [11] Guo H, Xu Y, Chen H, Zhou X. Thermodynamic characteristics of a novel supercritical

502 compressed air energy storage system. *Energy Convers Manage*, 2016;115:167-77.

503 [12] Oldenburg CM, Pan L. Porous media compressed-air energy storage (PM-CAES): theory and
504 simulation of the coupled wellbore-reservoir system. *Transport Porous Med* 2013;97(2): 201-
505 221

506 [13] Jannelli E, Minutillo M, Lavadera AL, Falcucci G. A small-scale CAES (compressed air energy
507 storage) system for stand-alone renewable energy power plant for a radio base station: a sizing-
508 design methodology. *Energy*, 2014;78:313-22.

509 [14] C.Bullough, C.Gatzen, C.Jakiel, M.Koller, A.Nowi, S.Zunft, Advanced adiabatic compressed
510 air energy storage for the integration of wnd, in: *European Wind Energy Conf. London, UK,*
511 2004.

512 [15] G. Grazzini, A.Milazzo, Thermodynamic analysis of CAES/TES system for renewable energy
513 plants, *Renew. Energy*, 33 (2008)1998-2006.

514 [16] W.F. Pickard, N.j. Hansing, A.Q. Shen, Can large-scale advanced-adiabatic compressed air
515 energy storage be justified economically in an age of sustainable energy, *J. Renew. Sustain.*
516 *Energy*, 1 (2009)033102:1-033102:10.

517 [17] Cárdenas, B., Pimm, A.J., Kantharaj, B., Simpson, M.C., Garvey, J.A. and Garvey, S.D., 2017.
518 Lowering the cost of large-scale energy storage: High temperature adiabatic compressed air
519 energy storage. *Propulsion and Power Research*, 6(2), pp.126-133.

520 [18] Szablowski, L., Krawczyk, P., Badyda, K., Karellas, S., Kakaras, E. and Bujalski, W., 2017.
521 Energy and exergy analysis of adiabatic compressed air energy storage system. *Energy*, 138,
522 pp.12-18

523 [19] He, W., Luo, X., Evans, D., Busby, J., Garvey, S., Parkes, D. and Wang, J., 2017. Exergy storage
524 of compressed air in cavern and cavern volume estimation of the large-scale compressed air
525 energy storage system. *Applied energy*, 208, pp.745-757.

526 [20] Guo, H., Xu, Y., Chen, H. and Zhou, X., 2016. Thermodynamic characteristics of a novel
527 supercritical compressed air energy storage system. *Energy conversion and management*, 115,
528 pp.167-177.

529 [21] Liu JL, Wang JH. A comparative research of two adiabatic compressed air energy storage
530 systems. *Energy Convers Manage*, 2016;108:566-78

531 [22] Yao E, Wang H, Wang L, Xi G, Marechal F. Thermo-economic optimization of a combined
532 cooling, heating and power system based on small-scale compressed air energy storage.
533 *Energy Convers Manage*, 2016; 118:377-86.

534 [23] Morgan, R., et al., Liquid air energy storage-Analysis and first results from a pilot scale
535 demonstration plant. *Applied Energy*, 2015. 137(3): p. 845-853.

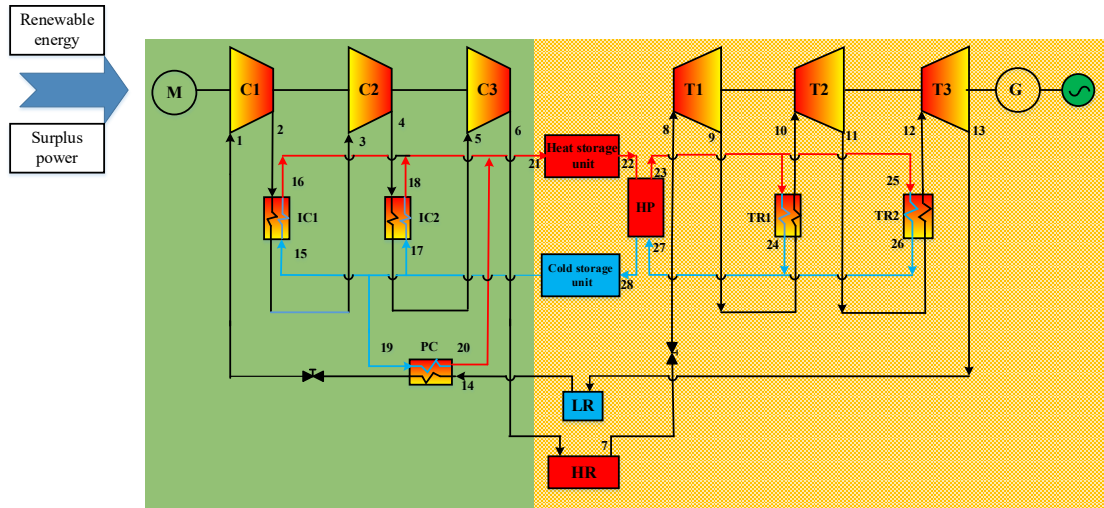
536 [24] HE Qing, WANG Lijian, ZHOU Qian, LU Chang, DU Dongmei, LIU Wenyi. Systematic
537 optimization and thermodynamic analysis of liquefied air energy storage system. *Energy*,
538 Vol.173, 2019.4.15: 162-173

539 [25] Wang M, Zhao P, Wu Y, Dai Y. Performance analysis of a novel energy storage system based
540 on liquid carbon dioxide. *Appl Therm Eng*, 2015; 91:812-23.

541 [26] Wu Y, Hu D, Wang M, Dai Y. A Novel Transcritical CO₂ Energy Storage System. *Journal of*
542 *Xi'an Jiao Tong University*, 2016.50 (3):45-49.

543 [27] Liu, H., He, Q., Borgia, A., Thermodynamic analysis of a compressed carbon dioxide energy
544 storage system using two saline aquifers at different depths as storage reservoirs. *Energy*
545 *Conversion and Management*, 2016. 127: p. 149-159.

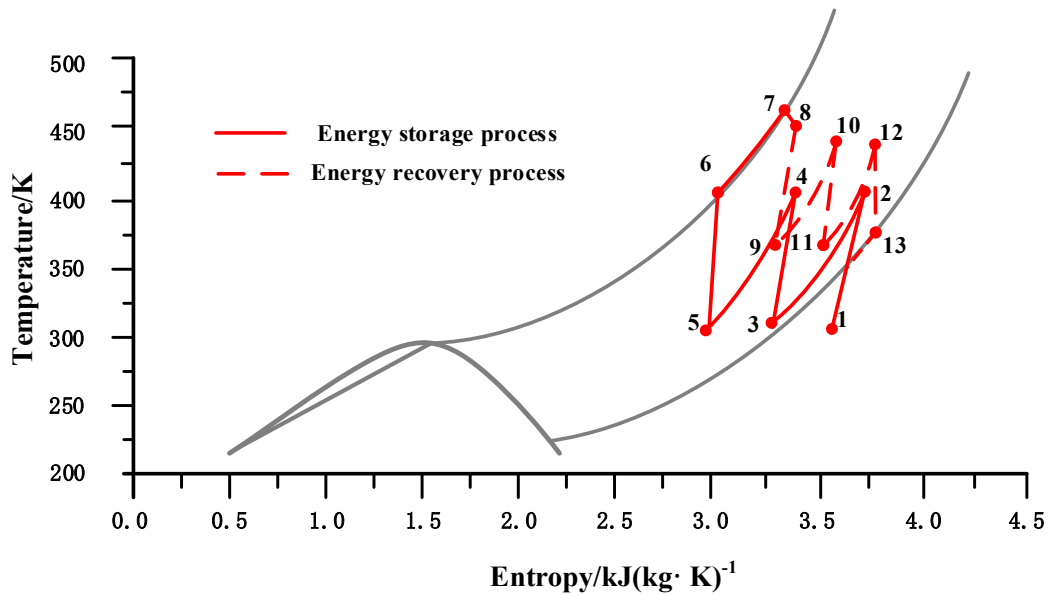
- 546 [28] Buscheck, T.A., Bielicki, J.M., Edmunds, T.A., Hao, Y., Sun, Y., Randolph, J.B. and Saar, M.O.
547 Multi-fluid geo-energy systems: Using geologic CO₂ storage for geothermal energy production
548 and grid-scale energy storage in sedimentary basins. *Geosphere*, 2016. 12(3), pp.678-696.
- 549 [29] Ahmadi M H, Mehrpooya M, Pourfayaz F. Thermodynamic and exergy analysis and
550 optimization of a transcritical CO₂ power cycle driven by geothermal energy with liquefied
551 natural gas as its heat sink[J]. *Applied Thermal Engineering*, 2016, 109:640-652.
- 552 [30] Ahmadi M H , Mehrpooya M , Pourfayaz F . Exergoeconomic analysis and multi objective
553 optimization of performance of a Carbon dioxide power cycle driven by geothermal energy
554 with liquefied natural gas as its heat sink[J]. *Energy Conversion and Management*, 2016,
555 119:422-434.
- 556 [31] Ahmadi M H, Mohammadi A, Pourfayaz F, et al. Thermodynamic analysis and optimization of
557 a waste heat recovery system for proton exchange membrane fuel cell using transcritical carbon
558 dioxide cycle and cold energy of liquefied natural gas[J]. *Journal of Natural Gas Science and
559 Engineering*, 2016, 34:428-438.
- 560 [32] Naseri A , Bidi M , Ahmadi M H , et al. Exergy Analysis of a hydrogen and water production
561 process by a solar-driven transcritical CO₂, power cycle with Stirling engine[J]. *Journal of
562 Cleaner Production*, 2017:S0959652617309228.
- 563 [33] Mercang Z M, Hemrle J, Kaufmann L, et al. Electrothermal energy storage with transcritical
564 CO₂ cycles[J]. *Energy*, 2012, 45(1):407-415.
- 565 [34] Zhang Y, Yang K, Hong H, et al. Thermodynamic analysis of a novel energy storage system
566 with carbon dioxide as working fluid[J]. *Renewable Energy*, 2016, 99:682-697.
- 567 [35] Zhang XR, Wang GB. Thermodynamic analysis of a novel energy storage system based on
568 compressed CO₂ fluid. *Int J Energy Res*, 2017; 41(10):1487-503.
- 569 [36] Arpagaus C, Bless F, Uhlmann M, et al. High temperature heat pumps: Market overview, state
570 of the art, research status, refrigerants, and application potentials[J]. *Energy*, 2018,
571 152:S0360544218305759.
- 572 [37] Huang M, Liang X, Zhuang R. Experimental investigate on the performance of high
573 temperature heat pump using scroll compressor. In:12th IEA Heat pump Cofferece,
574 Rotterdam;14-17 May,2017. P.1-8.
- 575 [38] NIST Standard Reference Database 23, NIST Thermodynamic and Transport Properties of
576 Refrigerants and Refrigerant Mixtures PEFPROP, Version 9.0, 2010.
- 577 [39] Sarkar J. Cycle parameter optimization of vortex tube expansion transcritical CO₂ system[J].
578 *International Journal of Thermal Science*, 2009, 48(9): 1823-1828.
- 579 [40] Succar, Samir, Williams Robert H. Compressed air energy storage: theory, resources, and
580 applications for wind power. Report no. 8. Princeton environmental institute; 2008.
- 581 [41] Kim YM, Lee JH, Kim SJ, Favrat D. Potential and evolution of compressed air energy storage:
582 energy and exergy analyses. *Entropy*, 2012;14(8):1501-21.
- 583 [42] Liu H, He Q, Saeed SB. Thermodynamic analysis of a compressed air energy storage system
584 through advanced exergetic analysis. *J Renew Sustain Energy*, 2016;8(3):034101.
- 585 [43] Wang L, Yang Y, Morosuk T, Tsatsaronis G. Advanced thermodynamic analysis and evaluation
586 of a supercritical power plant. *Energies*, 2012;5(6):1850-63.
- 587 [44] Qing H, Yinping H, Hui L, et al. Analysis of exergy efficiency of a super-critical compressed
588 carbon dioxide energy-storage system based on the orthogonal method[J]. *PLOS ONE*, 2018,
589 13(4):e0195614.



590

591

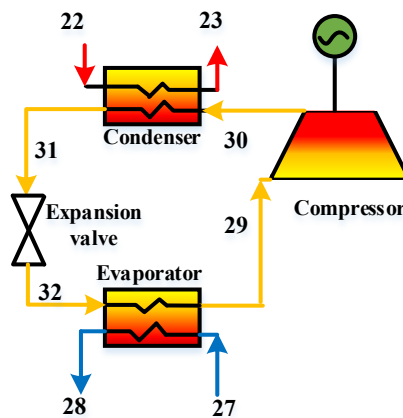
Fig. 1 Schematic of the TC-CCES system



592

593

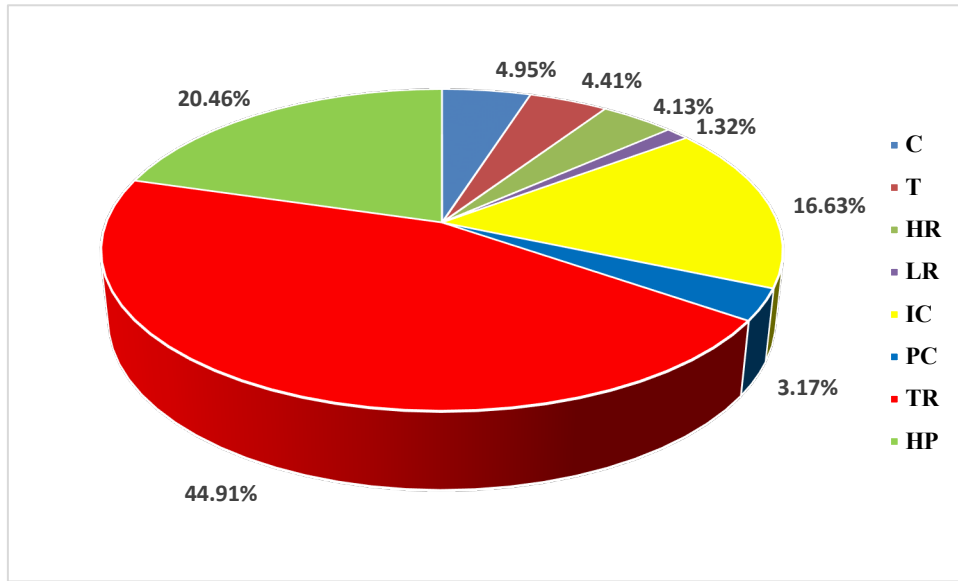
Fig. 2 T-S graph of the TC-CCES system



594

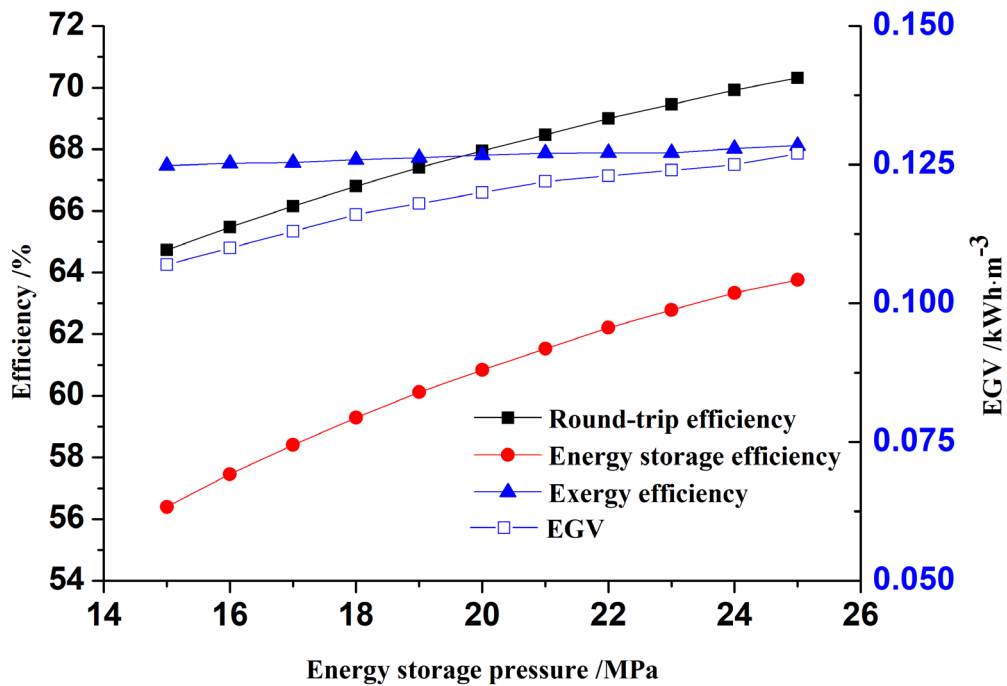
595

Fig. 3 Schematic of heat pump sub-system



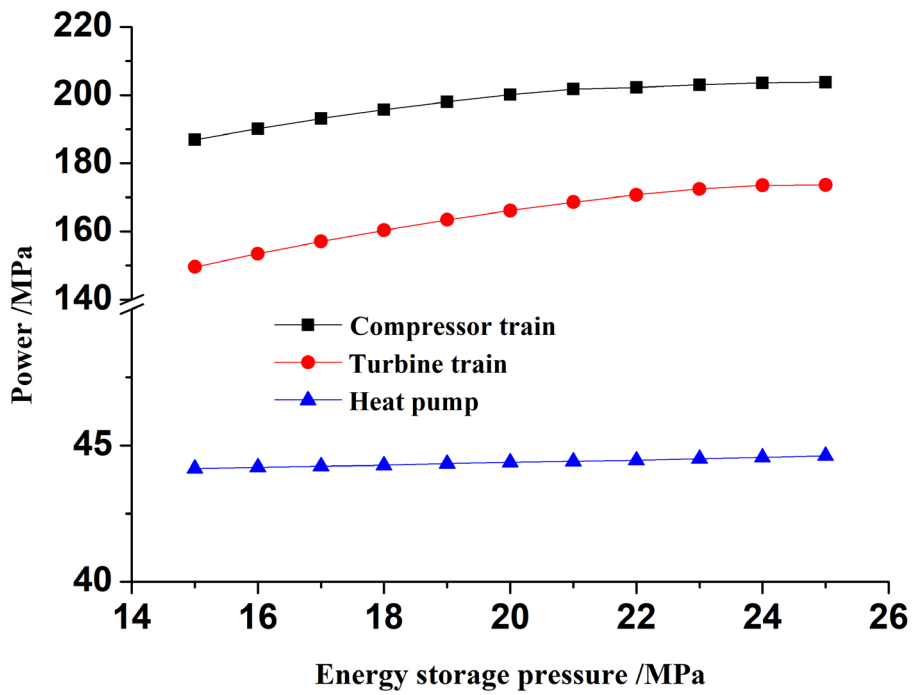
596
597
598
599
600

Fig. 4. The exergy destruction in the main components of the TC-CCES system.
C = compressor; T = turbine; HR = high-pressure reservoir; LR = low-pressure reservoir; IC = inter cooler of compressor; PC = pre-cooler; TR = turbine re-heater; HP = heat pump.



601
602

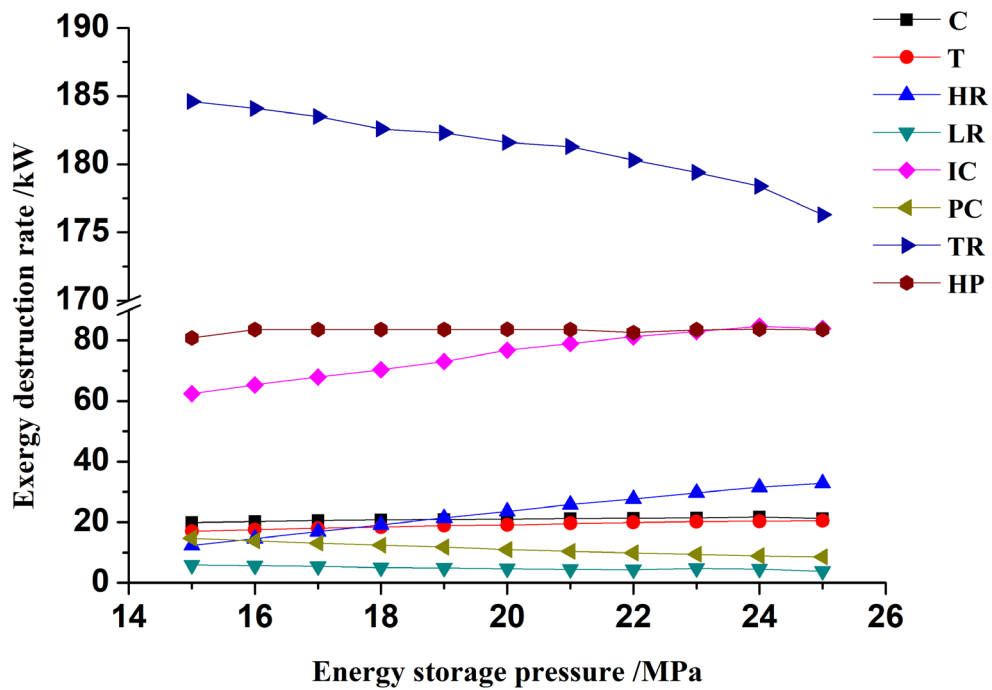
Fig. 5 Energy storage pressure control on system efficiency and EGV.



603

604

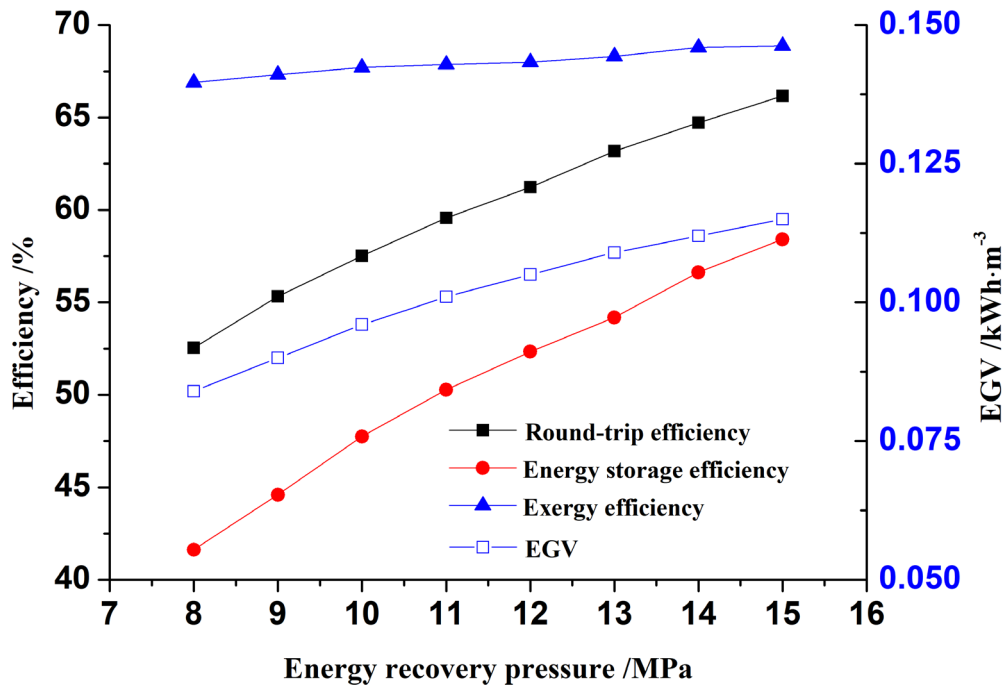
Fig. 6. Energy storage pressure control on power of compressor train, turbine train and heat pump



605

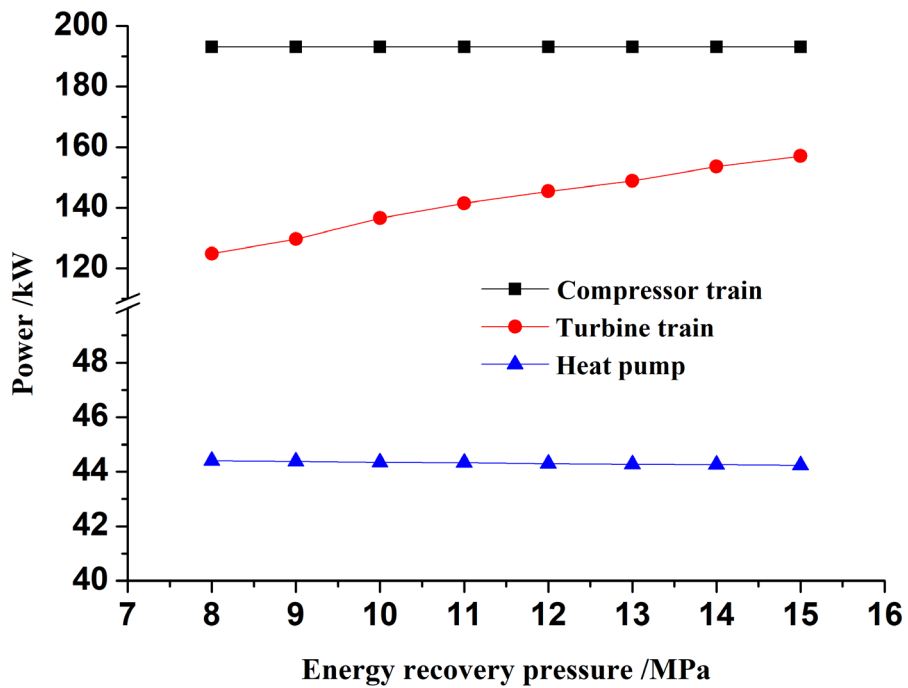
606

Fig. 7. Energy storage pressure control on exergy destruction rate.



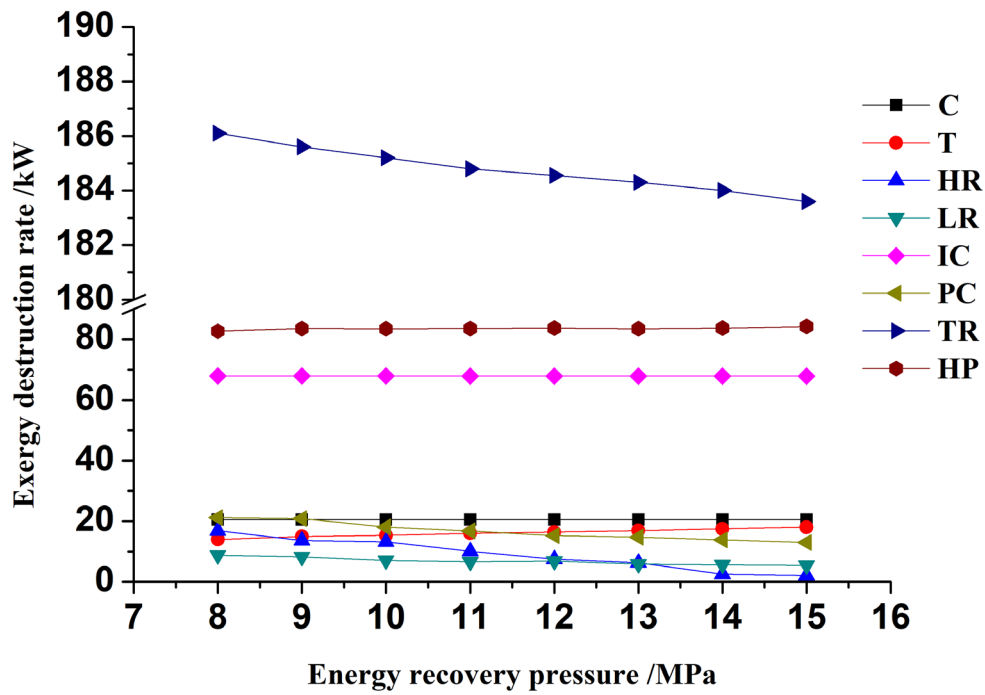
607
608

Fig. 8. Energy recovery pressure control on system efficiency and EGV.



609
610
611

Fig. 9. Energy recovery pressure control on power of compressor train, turbine train and heat pump.

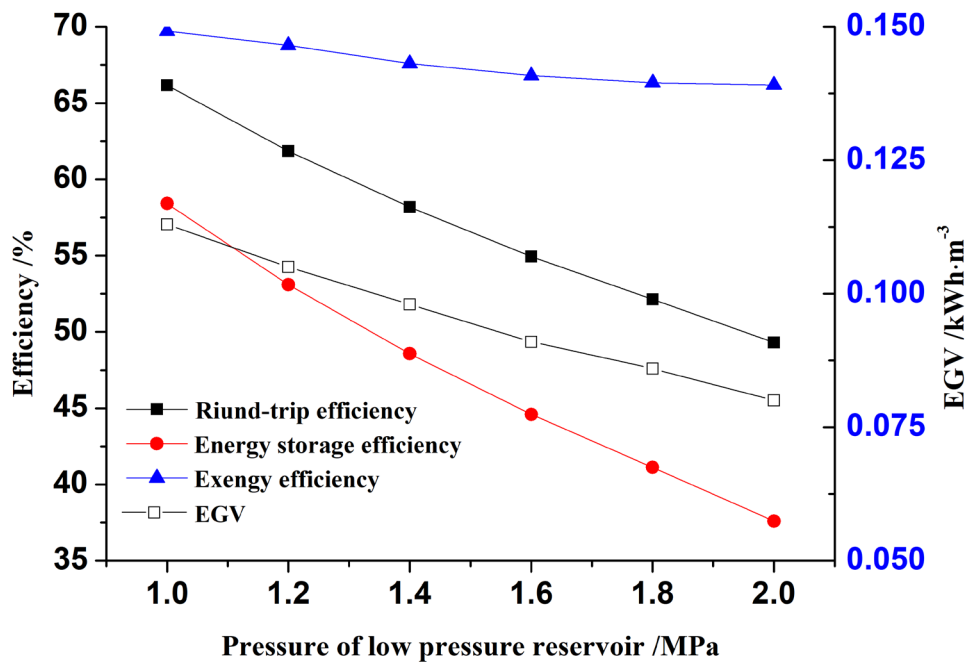


612

613

Fig. 10. Energy recovery pressure control on exergy destruction rate.

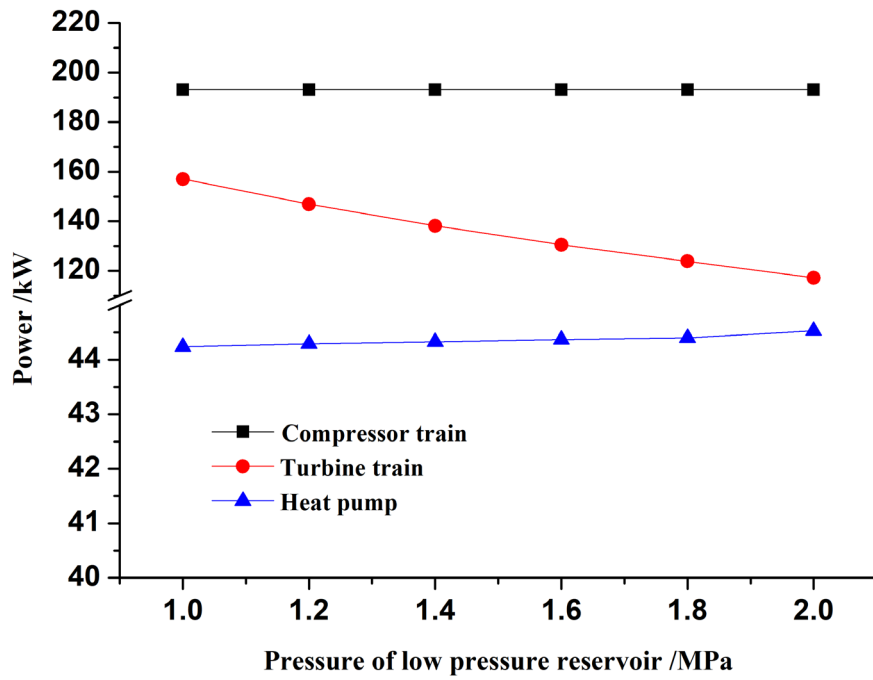
614



615

616

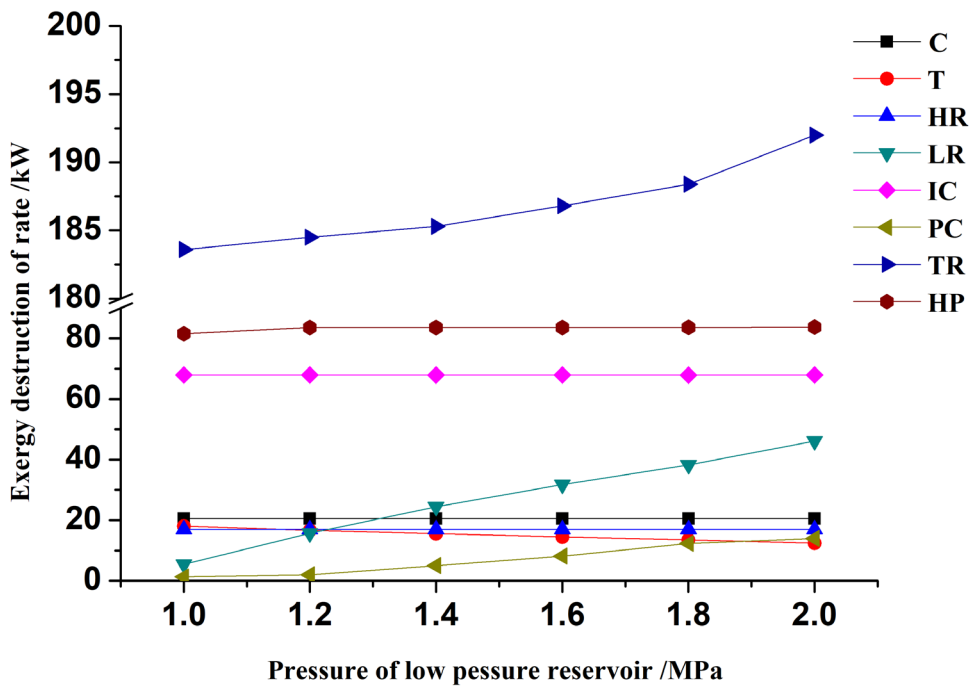
Fig. 11 Pressure of LR control on efficiency and EGV.



617

618

Fig. 12. Pressure of LR control on power of compressor train, turbine train and heat pump.



619

620

Fig. 13 Pressure of LR control on exergy destruction rate.

621

622

Table 1. Physical properties of R245fa.

Item	Value	Unit
Molecular formula	CHF ₂ CH ₂ CF ₃	
Critical temperature	427.15	K
Critical pressure	3.65	MPa
Boiling temperature	288.05	K

623

624

Table 2. Exergy calculation of components in the TC-CCES system

Component	$\dot{E}_{F,n}$	$\dot{E}_{P,n}$	$\dot{E}_{d,n}$
Compressor	W_c	$\dot{E}_c'' - \dot{E}_c'$	$\dot{E}_{F,c} - \dot{E}_{P,c}$
Turbine	$\dot{E}_T' - \dot{E}_T''$	W_T	$\dot{E}_{F,T} - \dot{E}_{P,T}$
Heat exchanger	$\dot{E}'_{hot,HE} - \dot{E}''_{hot,HE}$	$\dot{E}''_{cold,HE} - \dot{E}'_{cold,HE}$	$\dot{E}_{F,HE} - \dot{E}_{P,HE}$
Storage reservoir	\dot{E}'_{SC}	\dot{E}''_{SC}	$\dot{E}_{F,SC} - \dot{E}_{P,SC}$
Valve	\dot{E}'_V	\dot{E}''_V	$\dot{E}_{F,V} - \dot{E}_{P,V}$

625

626

Table 3. Properties of the TC-CCES system

Item	Value	Unit
Ambient temperature	298.15	K
Inlet temperature of compressor	308.15	K
Depth of LR	100	m
Depth of HR	1700	m
Throttle valve pressure drop in energy recovery process	0.2	MPa
Throttle valve pressure drop in energy storage process	2	MPa
Inlet temperature of cooling water	298.15	K
Inlet pressure of cooling water	0.2	MPa
Inlet pressure of compressor	0.8	MPa
Outlet pressure of the third stage compressor	17	MPa
Outlet pressure of the third stage turbine	1	MPa
Isentropic efficiency of compressor	86	%
Isentropic efficiency of turbine	88	%

627

Table 4. Material stream parameters of TC-CCES system

Stream No.	Temperature (K)	Pressure(MPa)	Mass flow rate (kg/h)
1	308.15	0.8	3600
2	395.85	2.216	3600
3	308.15	2.216	3600
4	399.95	6.138	3600
5	308.15	6.138	3600
6	396.85	17	3600
7	447.65	17	3600
8	441.75	15	3600
9	363.39	6.084	3600
10	423.15	6.084	3600
11	352.44	2.467	3600
12	423.15	2.467	3600
13	357.29	1	3600
14	361.29	1	3600
15	298.15	0.2	829.4
16	385.85	0.2	829.4
17	298.15	0.2	1110
18	389.95	0.2	1110
19	298.15	0.2	781.2
20	351.30	0.2	781.2
21	377.75	0.2	2721
22	377.75	0.1	3600
23	433.15	0.2	5164
24	406.35	0.1	5164
25	433.15	0.2	5540
26	407.45	0.1	5540
27	406.95	0.1	10700
28	363.15	0.1	3600
29	406.65	0.68	3600
30	435.85	1.7	3600
31	387.75	1.1	3600
32	377.05	0.3	3600

630

Table 5. Results of the main components in the TC-CCES

Term	Unit	Value
C1 power	kW	73.77
C2 power	kW	68.14
C3 power	kW	51.23
T1 power	kW	49.18
T2 power	kW	52.21
T3 power	kW	55.67
Heat pump power	kW	44.24

631

632

Table 6. Results of the performance criteria of the TC-CCES

Item	Unit	TC-CCES	Ref.[27]
Energy storage efficiency	%	58.41	20.04
Round-trip efficiency	%	66.00	63.35
Exergy efficiency	%	67.89	53.02
EGV	kW·h/m ³	2.12	3.07

633

634

Table 7. The power distribution in recovery process of the TC-CCES

Item	Unit	TC-CCES	Ref.[27]
Whole electricity output	kW	157.48	254.82
Extra fuel input	kW	0	217.86
Consume electricity	kW	44.24	0
Net electricity recovered from storage	kW	113.24	36.96

635

636

Table 8. Ranges of parameters for the sensitivity analysis

Parameters	Unit	Range
Energy storage pressure	MPa	16-25
Energy recovery pressure	MPa	8-15
Pressure of LR	MPa	1.0-2.0

637

Nomenclature

T	Temperature (K)
P	Pressure (MPa)
W	Power (kW)
E	Electricity power (kW·h)
\dot{Q}	Heat transfer rate (kW)
C_p	Specific heat capacity at constant pressure (kJ/(kg K))
G	Geothermal gradient (K/km)
\dot{m}	Mass flow rate (kg/h)
V	Volume (m ³)
Z	Reservoir depth (m)
t	Time (h)
Greek symbols	
Δ	Change quantity

η	Efficiency
ρ	Density (kg/m ³)
Subscripts	
T	Turbine
C	Compressor
<i>i</i>	Stage of compressor
<i>j</i>	Stage of turbine
'	Inlet stream
"	Outlet stream
Abbreviations	
CO ₂	Carbon dioxide
TC-CCES	Trans-critical compressed CO ₂ energy storage
CCES	Compressed CO ₂ energy storage
CAES	Compressed air energy storage
A-CAES	Adiabatic CAES
AA-CAES	Advanced adiabatic CAES
HP	Heat pump
HR	High-pressure reservoir
IC	Inner cooler exchanger
PC	Pre-cooler exchanger
TR	Turbine re-heater exchanger
C	Compressor
T	Turbine
LR	Low-pressure reservoir